A&A 526, A75 (2011)
DOI: 10.1051/0004-6361/201015460

Astronomy & Astrophysics

The period ratio for kink and sausage modes in a magnetic slab

C. K. Macnamara and B. Roberts

School of Mathematics and Statistics, University of St. Andrews, St. Andrews, Fife, KY16 9SS, Scotland
e-mail: cicely@mcs.st-andrews.ac.uk,br@st-and.ac.uk

Received 23 July 2010 / Accepted 23 November 2010

ABSTRACT

Aims. Increasing observational evidence of wave modes in the solar corona brings us to a closer understanding of that medium. Coronal seismology allows us to combine wave observations and theory to determine otherwise unknown parameters. The period ratio, $P_1/2P_2$, between the period P_1 of the fundamental mode and twice the period P_2 of its first overtone, is one such tool of coronal seismology and its departure from unity provides information about the structure of the corona.
Methods. We consider analytically the period ratio for the fast kink and sausage modes of a magnetic slab, discussing both an Epstein density profile and a simple step function profile.
Results. Transverse density structuring in the form of an Epstein profile or a step function profile may contribute to the shift of the period ratio for long thin slab-like structures.

Key words. Sun: corona – Sun: oscillations

1. Introduction

Observations of various coronal wave phenomena have become increasingly common in the literature within the last twenty years. From the launch of the Solar and Heliospheric Observatory (SoHO) and the Transition Region and Corona Explorer (TRACE) in the late 1990's to the present day, with new missions such as the Solar Dynamics Observatory (SDO) and *Hinode*, and instruments such as the Coronal Multi-Channel Polarimeter (CoMP) at Sacramento Peak Observatory, the evidence of waves in the solar corona is ever growing. Magnetoacoustic waves both slow and fast have been reported. Slow waves have been observed both as standing modes (Ofman et al. 1997; DeForest & Gurman 1998; Ofman et al. 1999; De Moortel et al. 2000, 2002a,b; Robbrecht et al. 2001; Ofman & Wang 2002; McEwan & De Moortel 2006; Marsh et al. 2009) and propagating modes (Wang et al. 2002, 2003, 2009; Srivastava & Dwivedi 2010). Standing fast waves are recorded in the form of transverse or vertical kink modes (Aschwanden et al. 1999, 2002; Nakariakov et al. 1999; Wang & Solanki 2004; Verwichte et al. 2004; Van Doorsselaere et al. 2007) or sausage modes (Nakariakov et al. 2003; Melnikov et al. 2005). Alfvénic or propagating kink waves have been reported by Tomczyk et al. (2007) and Tomczyk & McIntosh (2009), and interpreted by Van Doorsselaere et al. (2007) as propagating kink waves. Torsional Alfvén waves have been identified by Jess et al. (2009).

An increase in the observations of waves has led to an increased growth in the field of coronal seismology of magnetic loops, suggested over twenty five years ago by Roberts et al. (1984) who exploited the dispersion diagrams derived in Edwin & Roberts (1982, 1983). Coronal seismology helps to unveil the nature of the solar atmosphere; studying observed waves and drawing on their specific properties, it is possible to diagnose aspects of the coronal structure which might otherwise remain unknown. The period ratio between the fundamental mode and its first overtone has been noted as an effective tool for coronal seismology (Andries et al. 2005a,b; Goossens et al. 2006; McEwan et al. 2006, 2008; Donnelly et al. 2006; Dymova & Ruderman 2007; Díaz et al. 2007; Roberts 2008; Verth & Erdélyi 2008; Ruderman et al. 2008; Andries et al. 2009; Erdélyi & Morton 2009; Morton & Erdélyi 2009). This topic has recently been reviewed in Andries et al. (2009).

Observations of multi-periodicities (typically the fundamental mode and its first overtone) were first reported in standing fast waves (Verwichte et al. 2004; Van Doorsselaere et al. 2007; De Moortel & Brady 2007; O'Shea et al. 2007; Srivastava et al. 2008) and have very recently been found in slow modes (Srivastava & Dwivedi 2010). Using TRACE observations, Van Doorsselaere et al. (2007) found period ratios $P_1/P_2 = 1.81$ ($P_1/2P_2 = 0.91$), $P_1/P_2 = 1.58$ ($P_1/2P_2 = 0.79$) and $P_1/P_2 = 1.795$ ($P_1/2P_2 = 0.90$) for the fast kink mode. Using observations from the Solar Tower Telescope at Aryabhatta Research Institute of Observational Sciences, Srivastava et al. (2008) report a period ratio $P_1/P_2 = 1.68$ ($P_1/2P_2 = 0.84$) which has been attributed to the sausage mode. The observed tendency for the period ratio $P_1/2P_2$ between the fundamental mode of period P_1 and twice the period P_2 of its first overtone to be less than unity (the value for a simple wave on a string) has led to an interest in this ratio.

A number of physical effects have been assessed for their influence on the period ratio: wave dispersion, gravitational stratification, longitudinal and transverse density structuring, loop cross-sectional ellipticity, the overall geometry of a loop and magnetic field expansion (Andries et al. 2005a,b; McEwan et al. 2006, 2008; Díaz et al. 2007; Ruderman et al. 2008; Verth & Erdélyi 2008; Erdélyi & Morton 2009; Morton & Erdélyi 2009; Inglis et al. 2009). The overall conclusion seems to be that longitudinal structuring plays the most marked role (Andries et al. 2009). Longitudinal structuring may take the form of density stratification (e.g. Andries et al. 2005a,b; McEwan et al. 2006, 2008) or magnetic structuring (Verth & Erdélyi 2008).

In this work we consider analytically the behaviour of the period ratio for fast kink and sausage modes with transverse density structuring in the form of an Epstein profile. Previously transverse density structuring has been considered analytically in the form of a step function (Edwin & Roberts 1982, 1983), or as a smooth Epstein profile (Edwin & Roberts 1988) or its generalisation to a profile that combines both the step function and the Epstein profile through use of a free parameter (Nakariakov & Roberts 1995); the generalised case has to be treated numerically. Here we consider the Epstein profile as representative of a smoothly changing plasma density, providing a physically more realistic representation of density change than is given by the step function. The Epstein profile has been considered numerically in Pascoe et al. (2007, 2009), and the period ratio for the sausage mode has been determined numerically by Inglis et al. (2009). Our emphasis is on an analytical treatment of period ratios for the kink and sausage modes. We compare our results for the Epstein profile with the case of a simple magnetic slab with a step function density profile. The dispersion curves of a magnetic slab were given in Edwin & Roberts (1982, 1983); period ratios for such a slab have not hitherto been discussed. Our treatment is entirely in a cartesian geometry; we do not consider the case of a cylindrical tube (which requires a separate, probably numerical, treatment).

2. Model

We consider a magnetic slab aligned with the z-axis of a cartesian coordinate system $Oxyz$. The equilibrium magnetic field is $B_0\boldsymbol{e}_z$ and is taken to be uniform. Across the magnetic field, the equilibrium plasma density is $\rho_0(x)$; this produces a non-uniform Alfvén speed $c_{\rm A}(x) = (B_0^2/\mu\rho_0(x))^{1/2}$ which varies across the magnetic field. The slab is of length $2L$ with its ends at $z = \pm L$; we consider the slab to be anchored at its ends (modelling line tying of a coronal loop by the photosphere). Both gravity and acoustic effects are not considered.

We take the following set of ideal zero-β MHD equations:

$$\rho\left(\frac{\partial \boldsymbol{v}}{\partial t} + (\boldsymbol{v}\cdot\boldsymbol{\nabla})\boldsymbol{v}\right) = \frac{1}{\mu}(\nabla\times\boldsymbol{B})\times\boldsymbol{B}, \tag{1}$$

$$\frac{\partial \boldsymbol{B}}{\partial t} = \nabla\times(\boldsymbol{v}\times\boldsymbol{B}), \qquad \nabla\cdot\boldsymbol{B} = 0, \tag{2}$$

$$\frac{\partial \rho}{\partial t} + \nabla\cdot(\rho\boldsymbol{v}) = 0. \tag{3}$$

The set of ideal MHD Eqs. (1)–(3) are linearised about the non-uniform equilibrium density $\rho_0(x)$ embedded within the uniform field $B_0\boldsymbol{e}_z$. The linearised form of Eq. (3) gives the resulting density perturbations. We take the perturbed motions to be $\boldsymbol{v} = (v_x, v_y, 0)$, there being no force in the direction of the applied magnetic field in a zero-β plasma ($v_z = 0$). Then the linearised form of Eqs. (1) and (2) may be manipulated to yield the coupled partial differential equations

$$\frac{1}{c_{\rm A}^2(x)}\frac{\partial^2 v_x}{\partial t^2} - \frac{\partial^2 v_x}{\partial z^2} = \frac{\partial}{\partial x}\left(\frac{\partial v_x}{\partial x} + \frac{\partial v_y}{\partial y}\right) \tag{4}$$

$$\frac{1}{c_{\rm A}^2(x)}\frac{\partial^2 v_y}{\partial t^2} - \frac{\partial^2 v_y}{\partial z^2} = \frac{\partial}{\partial y}\left(\frac{\partial v_x}{\partial x} + \frac{\partial v_y}{\partial y}\right). \tag{5}$$

In a uniform medium Eqs. (4) and (5) describe the Alfvén and fast magnetoacoustic waves of a zero-β plasma. Here we are interested in the fast waves in a non-uniform medium; accordingly, we suppose that $v_y = 0$ and $\partial/\partial y = 0$ so that the perturbed motions $\boldsymbol{v} = (v_x, 0, 0)$ are perpendicular to the applied magnetic field and lie entirely in the plane of the density non-uniformity. These motions are compressible. Equations (4) and (5) then give the wave equation

$$\frac{\partial^2 v_x}{\partial t^2} = c_{\rm A}^2(x)\left(\frac{\partial^2 v_x}{\partial x^2} + \frac{\partial^2 v_x}{\partial z^2}\right). \tag{6}$$

Finally, setting

$$v_x(x,z,t) = v_x(x)\mathrm{e}^{\mathrm{i}(\omega t - k_z z)} \tag{7}$$

for frequency ω and wavenumber k_z, we obtain the ordinary differential equation

$$\frac{\mathrm{d}^2 v_x}{\mathrm{d}x^2} + \left(\frac{\omega^2}{c_{\rm A}^2(x)} - k_z^2\right)v_x = 0. \tag{8}$$

The generalisation of (8) to include acoustic effects (non-zero β) and also three dimensional motions is given in Roberts (1981).

We are particularly interested in the Epstein profile for the equilibrium plasma density

$$\rho_0(x) = \rho_{\rm e} + (\rho_0 - \rho_{\rm e})\mathrm{sech}^2\left(\frac{x}{a}\right), \tag{9}$$

where ρ_0 and $\rho_{\rm e}$ are the internal and external densities respectively and a is the spatial scale over which the density varies. This profile provides a smooth representation of a physically realistic situation. The density varies smoothly from ρ_0 at $x = 0$ to $\rho_{\rm e}$ as $x \to \pm\infty$. The corresponding Alfvén speeds are $c_{\rm A0} = (B_0^2/\mu\rho_0)^{1/2}$ at $x = 0$ and $c_{\rm Ae} = (B_0^2/\mu\rho_{\rm e})^{1/2}$ as $x \to \pm\infty$; thus $\rho_0 c_{\rm A0}^2 = \rho_{\rm e} c_{\rm Ae}^2$. The Epstein profile is a convenient model for both analytical (Edwin & Roberts 1988; Nakariakov & Roberts 1995) and numerical (Cooper et al. 2003; Pascoe et al. 2007; Inglis et al. 2009) studies. The Epstein profile may also be compared with the simple step function profile of a magnetic slab investigated in Edwin & Roberts (1982, 1983).

Following Landau & Lifshitz (1958), we solve Eq. (8) in terms of hypergeometric functions and find the solution

$$v_x = (1-s^2)^{\lambda/2}F(A,B,C,(1-s)/2) \tag{10}$$

where $s = \tanh(x/a)$, $A = \lambda - \nu$, $B = 1 + \lambda + \nu$, $C = 1 + \lambda$ for λ and ν given by

$$\lambda = k_z a\left(1 - \frac{c^2}{c_{\rm Ae}^2}\right)^{1/2} \tag{11}$$

and

$$\nu(\nu+1) = k_z^2 a^2\left(\frac{c^2}{c_{\rm A0}^2} - \frac{c^2}{c_{\rm Ae}^2}\right). \tag{12}$$

The hypergeometric function F is defined by (Abramowitz & Stegun 1965)

$$F(A,B,C,(1-s)/2) = \sum_{m=0}^{n}\frac{(A)_m(B)_m}{(C)_m}\left(\frac{1-s}{2}\right)^m \tag{13}$$

where

$$(\alpha)_m = \frac{\Gamma(\alpha+m)}{\Gamma(\alpha)} \tag{14}$$

and $\Gamma(\alpha)$ denotes the gamma function of argument α. The dispersion relation is given by

$$\nu = \lambda + n, \qquad \text{for } n = 0, 1, 2, \ldots \tag{15}$$

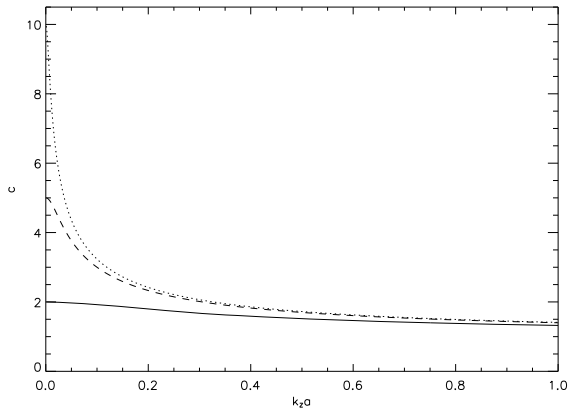

Fig. 1. A plot of the wave speed c (in units of c_{A0}) with respect to $k_z a$ for $c_{Ae}/c_{A0} = (\rho_0/\rho_e)^{1/2} = 2, 5$, and 10 for the solid, dashed, and dotted curves respectively. The speed c is bounded below by c_{A0} and above by c_{Ae}.

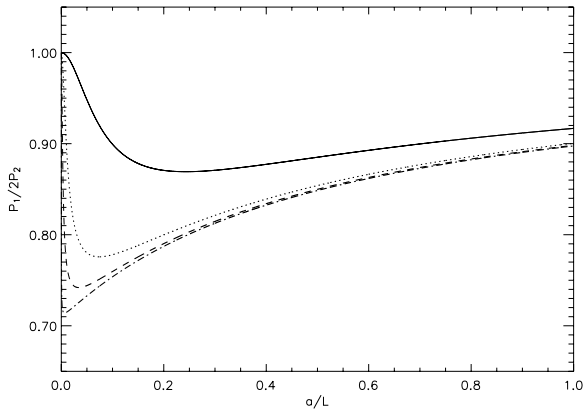

Fig. 2. A plot of the period ratio $P_1/2P_2$ with respect to a/L for the fast kink mode with an Epstein density profile and $c_{Ae}/c_{A0} = 2, 5, 10$, and 50 for the solid, dotted, dashed and dot-dashed curves respectively.

3. The kink mode

In the case of the fast kink mode ($n = 0$), which disturbs the central axis of the loop (the z-axis), so $v_x \neq 0$ at $x = 0$, Eq. (8) has the solution

$$v_x = v_0 \left[\operatorname{sech}\left(\frac{x}{a}\right)\right]^{\lambda}, \tag{16}$$

for arbitrary amplitude v_0. The power λ is determined transcendentally through the dispersion relation $\lambda = \nu$. The dispersion relation $\lambda = \nu$ implies that

$$k_z a = \frac{\left(c_{Ae}^2 - c^2\right)}{\left(c^2 - c_{A0}^2\right)}^{1/2} \frac{c_{A0}^2}{c_{Ae}}. \tag{17}$$

This relation has been given by Cooper et al. (2003).

Equation (17) determines the wave speed c ($= \omega/k_z$) as a function of $k_z a$. In order that $k_z a$ is real and positive we require $c_{A0} < c < c_{Ae}$. We note that for $k_z a \to 0$ Eq. (17) leads to $c = c_{Ae}$, and for $k_z a \to \infty$, $c = c_{A0}$. Further, for $c_{Ae} \gg c_{A0}$ Eq. (17) yields

$$c^2 = c_{A0}^2 \left(1 + \frac{1}{k_z a}\right). \tag{18}$$

Equation (18) provides an upper bound on the behaviour of c^2. The limit $c_{Ae} \to \infty$ described by (18) applies if $\rho_e \to 0$, i.e. the environment is a vacuum.

The general solution of the kink dispersion relation (17) for the square of the wave speed is given by

$$c^2 = \frac{c_{A0}^2}{2c_{Ae}^2 k_z^2 a^2}\left(2c_{Ae}^2 k_z^2 a^2 - c_{A0}^2 + \sqrt{c_{A0}^4 + 4c_{Ae}^4 k_z^2 a^2 - 4c_{A0}^2 c_{Ae}^2 k_z^2 a^2}\right). \tag{19}$$

We plot this solution in Fig. 1. The behaviour of the solution is such that as $k_z a$ increases c decreases from c_{Ae} to c_{A0} and so we expect the period ratio to be less than unity.

3.1. The period ratio for the kink mode

For a loop of length $2L$, the wavenumber k_z is taken as $k_z = \pi/2L$ for the fundamental mode and $k_z = \pi/L$ for the first overtone. Thus the speed c_1 of the fundamental mode is given by Eq. (19) and the frequency is given by $\omega_1 = k_z c_1$ where $k_z = \pi/2L$. The speed c_2 of the first overtone is given by Eq. (19) and the frequency is given by $\omega_2 = k_z c_2$ where $k_z = \pi/L$. We use the subscript 1 to denote any value pertaining to the fundamental mode and the subscript 2 to denote the first overtone. The fundamental period is given by $P_1 = 2\pi/\omega_1 = 4L/c_1$ and the period of the first overtone is $P_2 = 2\pi/\omega_2 = 2L/c_2$. Thus the period ratio determined by the dispersion relation (17) is $P_1/2P_2 = c_2/c_1$ where c_1 and c_2 are determined from Eq. (19):

$$\left(\frac{P_1}{2P_2}\right)^2 = \frac{1}{4}\left(\frac{2\frac{\pi^2 a^2}{L^2} - \frac{c_{A0}^2}{c_{Ae}^2} + \sqrt{\frac{c_{A0}^4}{c_{Ae}^4} + 4\frac{\pi^2 a^2}{L^2} - 4\frac{c_{A0}^2}{c_{Ae}^2}\frac{\pi^2 a^2}{L^2}}}{\frac{\pi^2 a^2}{2L^2} - \frac{c_{A0}^2}{c_{Ae}^2} + \sqrt{\frac{c_{A0}^4}{c_{Ae}^4} + \frac{\pi^2 a^2}{L^2} - \frac{c_{A0}^2}{c_{Ae}^2}\frac{\pi^2 a^2}{L^2}}}\right). \tag{20}$$

Regardless of the values of the internal and external Alfvén speeds (c_{A0} and c_{Ae}), as $a/L \to \infty$ the period ratio is unity. Thus for long thin loops the period ratio is unaffected by transverse density structuring in the form of the Epstein profile.

In Fig. 2 we plot the period ratio for the kink mode under an Epstein profile for selected values of c_{Ae}/c_{A0}. For all values of c_{Ae}/c_{A0}, in the limits $a/L \to 0$ and $a/L \to \infty$ the period ratio is unity. Thus for long and thin or short and fat loops the period ratio is close to unity. For small a/L there is a rapid departure from unity, possibly falling to as low a value as $P_1/2P_2 = 1/\sqrt{2}$ in the limit of $c_{Ae} \gg c_{A0}$. This tendency towards a least value is shown in Fig. 3 where we plot the minimum value of the period ratio as a function of c_{Ae}/c_{A0}.

3.2. Approximations for small and large a/L

Consider Eq. (19) in the extreme $2c_{Ae}^2 k_z^2 a^2 \gg c_{A0}^2$, which applies for all $k_z a$ as $c_{Ae}/c_{A0} \to \infty$ and for all c_{Ae}/c_{A0} as $k_z a \to \infty$. We consider this approximation for $k_z a \to \infty$ (corresponding to $a/L \to \infty$). With $2c_{Ae}^2 k_z^2 a^2 \gg c_{A0}^2$, Eq. (19) yields

$$c^2 = c_{A0}^2 \left(1 + \frac{\mu_1}{k_z a}\right) \tag{21}$$

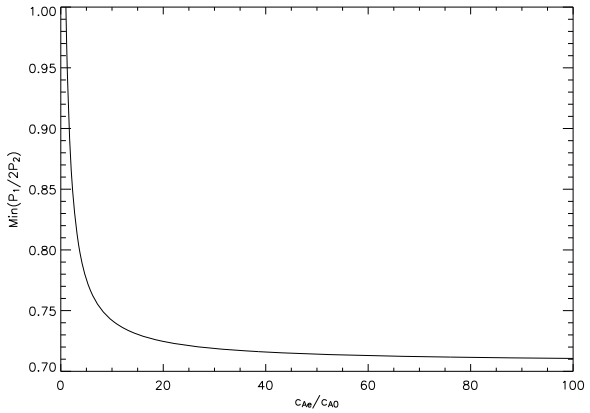

Fig. 3. A plot of the minimum value of the period ratio $P_1/2P_2$ for the kink mode with respect to $c_{\rm Ae}/c_{\rm A0} = (\rho_0/\rho_{\rm e})^{1/2}$. In the extreme $c_{\rm Ae}/c_{\rm A0} \to \infty$, the period ratio minimum approaches $\sqrt{1/2}$.

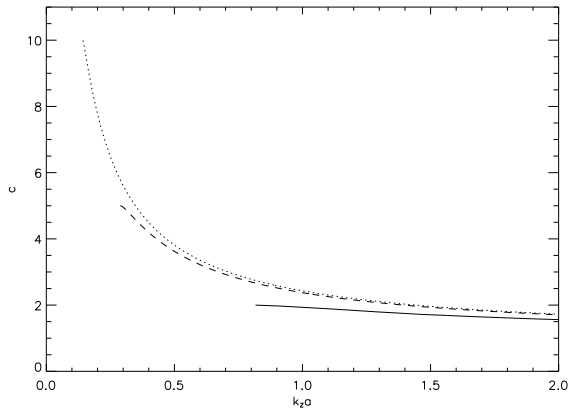

Fig. 4. A plot of the wave speed c (in units of $c_{\rm A0}$) with respect to $k_z a$ for $c_{\rm Ae}/c_{\rm A0} = 2, 5$, and 10 shown as solid, dashed, and dotted curves respectively. The cutoff value for each curve is given by Eq. (30). For example, the curve with $c_{\rm Ae}/c_{\rm A0} = 2$ has a cutoff of $k_z a = \sqrt{2/3}$.

where

$$\mu_1 = \left(\frac{c_{\rm Ae}^2 - c_{\rm A0}^2}{c_{\rm Ae}^2}\right)^{1/2}, \quad 0 < \mu_1 < 1. \tag{22}$$

The period ratio is then given by

$$\frac{P_1}{2P_2} = \left(\frac{1 + \dfrac{\mu_1 L}{\pi a}}{1 + \dfrac{2\mu_1 L}{\pi a}}\right)^{1/2}. \tag{23}$$

For $c_{\rm Ae} \gg c_{\rm A0}$, $\mu_1 = 1$ and Eq. (23) gives $P_1/2P_2 = 1$ for $a/L \to \infty$ and $P_1/2P_2 = 1/\sqrt{2}$ for $a/L \to 0$, in agreement with Figs. 2 and 3. Expanding Eq. (23) gives

$$\frac{P_1}{2P_2} = 1 - \frac{\mu_1 L}{2\pi a} + \frac{7\mu_1^2 L^2}{8\pi^2 a^2} + \ldots, \qquad \frac{\pi a}{2L} \gg 1. \tag{24}$$

In the opposite extreme of $\pi a/2L \ll 1$, the period ratio is given by

$$\frac{P_1}{2P_2} = 1 - \frac{3\pi^2 a^2 \mu_2}{8L^2} - \frac{21\pi^4 a^4 \mu_2^2}{128 L^4} + \ldots, \qquad \frac{\pi a}{2L} \ll 1, \tag{25}$$

where

$$\mu_2 = \left(\frac{c_{\rm Ae}^2 - c_{\rm A0}^2}{c_{\rm A0}^2}\right)^2. \tag{26}$$

We note that as $a/L \to 0$ the period ratio is unity.

4. The sausage mode

In the case of the sausage mode ($n = 1$) Eq. (8) has solution

$$v_x(x) = v_0 \tanh\left(\frac{x}{a}\right)\left[\operatorname{sech}\left(\frac{x}{a}\right)\right]^{\lambda}, \tag{27}$$

for arbitrary amplitude v_0, giving $v_x = 0$ at $x = 0$. From Eqs. (11) and (12), the dispersion relation $\nu = 1 + \lambda$ gives

$$k_z^2 a^2 \left(\frac{c^2}{c_{\rm A0}^2} - 1\right) - 3k_z a \left(1 - \frac{c^2}{c_{\rm Ae}^2}\right)^{1/2} - 2 = 0. \tag{28}$$

Relation (28) has been given in Cooper et al. (2003); see also Pascoe et al. (2007) and Inglis et al. (2009). The presence of the square root in (28) makes it clear that we require $c^2 \le c_{\rm Ae}^2$. Moreover, since $1 - c^2/c_{\rm Ae}^2 \le 1$, it follows from (28) that the wave speed squared is bounded above by the expression

$$c^2 = c_{\rm A0}^2 \left(1 + \frac{3}{k_z a} + \frac{2}{k_z^2 a^2}\right). \tag{29}$$

In fact, this bound is achieved in the limit $c_{\rm Ae} \to \infty$, which attains whenever $\rho_{\rm e} \to 0$, i.e. if the environment is a vacuum. The bound (29) shows that $c^2 \to c_{\rm A0}^2$ as $k_z a \to \infty$, so altogether the solutions of (28) satisfy $c_{\rm A0}^2 \le c^2 \le c_{\rm Ae}^2$.

The upper bound (29) is not a strong constraint for small $k_z a$. In fact it is evident from the dispersion relation (28) that when $c^2 = c_{\rm Ae}^2$ we require

$$k_z a = \left(\frac{2c_{\rm A0}^2}{c_{\rm Ae}^2 - c_{\rm A0}^2}\right)^{1/2}, \qquad \text{cutoff;} \tag{30}$$

$k_z a$ must exceed this cutoff value.

The dispersion relation (28) may be viewed as a quadratic equation determining $k_z a$ as a function of $c/c_{\rm A0}$ for given $c_{\rm Ae}/c_{\rm A0}$ $(= (\rho_0/\rho_{\rm e})^{1/2})$. Specifically,

$$k_z a = \frac{3\left(1 - \dfrac{c^2}{c_{\rm Ae}^2}\right)^{1/2} + \left(1 - 9\dfrac{c^2}{c_{\rm Ae}^2} + 8\dfrac{c^2}{c_{\rm A0}^2}\right)^{1/2}}{2\left(\dfrac{c^2}{c_{\rm A0}^2} - 1\right)}, \tag{31}$$

the second root of the quadratic being rejected (it gives $k_z a < 0$).

We may also solve (28) for the square of the wave speed, viz.

$$c^2 = \frac{c_{\rm A0}^2}{2c_{\rm Ae}^2 k_z^2 a^2}\left(2c_{\rm Ae}^2 k_z^2 a^2 + 4c_{\rm Ae}^2 - 9c_{\rm A0}^2 + 3\sqrt{9c_{\rm A0}^4 - 4c_{\rm A0}^2 c_{\rm Ae}^2 k_z^2 a^2 - 8c_{\rm A0}^2 c_{\rm Ae}^2 + 4c_{\rm Ae}^4 k_z^2 a^2}\right). \tag{32}$$

We plot this solution in Fig. 4 as a function of $k_z a$. The behaviour of the solution is such that the speed c exists for values of $k_z a$ above the cutoff (30) after which as $k_z a$ increases c decreases and so we expect the period ratio to be less than unity. Increasing the ratio $c_{\rm Ae}/c_{\rm A0}$ between the internal and external Alfvén speeds acts to increase the speed c for a particular $k_z a$.

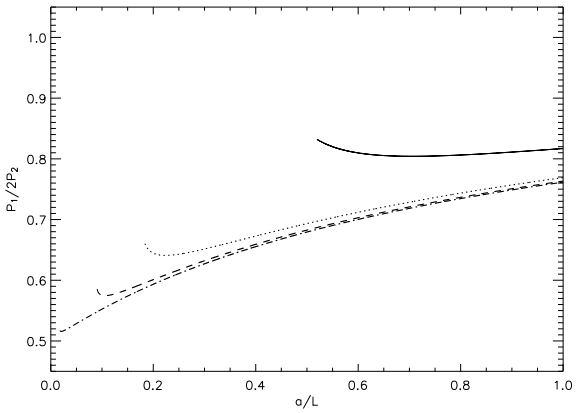

Fig. 5. A plot of the period ratio $P_1/2P_2$ with respect to a/L for the fast sausage mode with an Epstein density profile for $c_{\rm Ae}/c_{\rm A0} = 2, 5, 10$ and 50 for the solid, dotted, dashed and dot-dashed curves respectively.

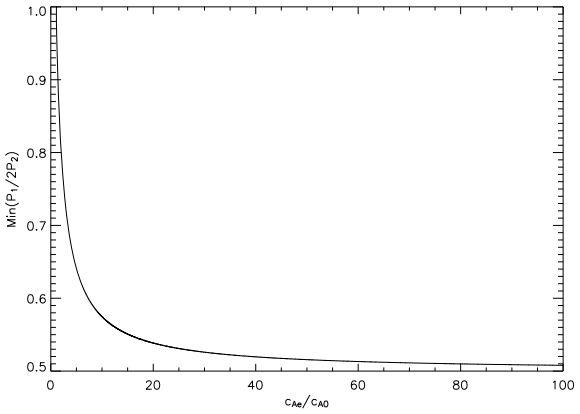

Fig. 6. A plot of the minimum value of the period ratio $P_1/2P_2$ for the sausage mode with respect to $c_{\rm Ae}/c_{\rm A0}$. In the extreme $c_{\rm Ae}/c_{\rm A0} \to \infty$, the period ratio minimum approaches 1/2.

4.1. The period ratio for the sausage mode

The period ratio for the sausage mode is given by $P_1/2P_2 = c_2/c_1$ where c_1 and c_2 are determined by (32). Thus the period ratio is determined by

$$\left(\frac{P_1}{2P_2}\right)^2 = \frac{1}{4}\left\{\frac{4+2\frac{\pi^2a^2}{L^2}-9\frac{c_{\rm A0}^2}{c_{\rm Ae}^2}+3\sqrt{9\frac{c_{\rm A0}^4}{c_{\rm Ae}^4}-4\frac{c_{\rm A0}^2}{c_{\rm Ae}^2}\frac{\pi^2a^2}{L^2}-8\frac{c_{\rm A0}^2}{c_{\rm Ae}^2}+4\frac{\pi^2a^2}{L^2}}}{4+\frac{\pi^2a^2}{2L^2}-9\frac{c_{\rm A0}^2}{c_{\rm Ae}^2}+3\sqrt{9\frac{c_{\rm A0}^4}{c_{\rm Ae}^4}-\frac{c_{\rm A0}^2}{c_{\rm Ae}^2}\frac{\pi^2a^2}{L^2}-8\frac{c_{\rm A0}^2}{c_{\rm Ae}^2}+\frac{\pi^2a^2}{L^2}}}\right\}. \tag{33}$$

In the limit $a/L \to \infty$ the period ratio $P_1/2P_2 \to 1$. In Fig. 5 we plot the period ratio for the sausage mode under the Epstein profile. A similar graph is given in Inglis et al. (2009).

Just as in the case of the kink mode we note that the period ratio appears to have a limit of 1/2 as $c_{\rm Ae}/c_{\rm A0} \to \infty$ and $a/L \to 0$. We plot in Fig. 6 the minimum value of the period ratio with respect to $c_{\rm Ae}/c_{\rm A0}$ and note that as $c_{\rm Ae}/c_{\rm A0} \to \infty$ the minimum value approaches 1/2.

4.2. Approximation for large a/L

As for the kink mode we consider the approximation for $2c_{\rm Ae}^2k_z^2a^2 \gg c_{\rm A0}^2$, corresponding to the ratio $c_{\rm Ae}/c_{\rm A0}$ being much greater than L/a. This gives

$$c^2 = c_{\rm A0}^2\left(1+\frac{3\mu_1}{k_za}+\frac{2}{k_z^2a^2}\right), \tag{34}$$

where μ_1 is given by Eq. (22) as for the kink mode case. The period ratio is then given by

$$\frac{P_1}{2P_2} = \left(\frac{1+\frac{3\mu_1L}{\pi a}+\frac{2L^2}{\pi^2a^2}}{1+\frac{6\mu_1L}{\pi a}+\frac{8L^2}{\pi^2a^2}}\right)^{1/2}. \tag{35}$$

For $c_{\rm Ae} \gg c_{\rm A0}$, $\mu_1 = 1$ and Eq. (35) gives $P_1/2P_2 \to 1/2$ for $a/L \to 0$, although this may not be attained due to the cutoff, and $P_1/2P_2 \to 1$ for $a/L \to \infty$. Expanding Eq. (35) we obtain

$$\frac{P_1}{2P_2} = 1-\frac{3\mu_1L}{2\pi a}-\frac{3L^2}{\pi^2a^2}+\frac{63\mu_1^2L^2}{8\pi^2a^2}+\ldots, \quad \frac{\pi a}{2L} \gg 1. \tag{36}$$

5. Comparison between the Epstein profile and a step function slab

The results for the Epstein profile show how period ratios vary with the density ratio $\rho_0/\rho_{\rm e}$ (or equivalently $(c_{\rm Ae}/c_{\rm A0})^{1/2}$) and the length L of the magnetic field lines. It is natural to compare these results with the simpler magnetic slab model of a step function change in the plasma density. Dispersion curves for the step function slab are well known (see Edwin & Roberts 1982, 1983) but hitherto period ratios have not been determined. We give a brief discussion here.

The starting point for our discussion is again the wave Eq. (8), but now in place of the Epstein profile (9) we consider the step function

$$\rho_0(x) = \begin{cases} \rho_{\rm e}, & |x| > a, \\ \rho_0, & |x| < a, \end{cases} \tag{37}$$

the internal density ρ_0 changing to $\rho_{\rm e}$ discontinuously at the slab boundaries at $x = \pm a$. Following the notation of Edwin & Roberts (1982), we write

$$n_0^2 = \frac{\omega^2}{c_{\rm A0}^2}-k_z^2, \qquad m_{\rm e}^2 = k_z^2-\frac{\omega^2}{c_{\rm Ae}^2} \tag{38}$$

where $c_{\rm A0}$ is the Alfvén speed in the slab ($-a < x < a$) and $c_{\rm Ae}$ is the Alfvén speed in the environment ($|x| > a$). Equation (8) has solution

$$v_x(x) = \begin{cases} \alpha_{\rm e}{\rm e}^{-m_{\rm e}(x-a)}, & x > a \\ \alpha_0\cos n_0x+\beta_0\sin n_0x, & |x| < a \\ \beta_{\rm e}{\rm e}^{m_{\rm e}(x+a)}, & x < -a. \end{cases} \tag{39}$$

In order that the velocity disturbance is effectively confined to the interior of the slab, so that $v_x \to 0$ as $|x| \to \infty$, we require $m_{\rm e} > 0$. It is also required (see Roberts 1981; Edwin & Roberts 1982) that both v_x and the total pressure perturbation p_T are continuous at $x = \pm a$, where

$$p_T(x) = \frac{{\rm i}\rho_0}{\omega}c_{\rm A}^2(x)\frac{{\rm d}v_x}{{\rm d}x}. \tag{40}$$

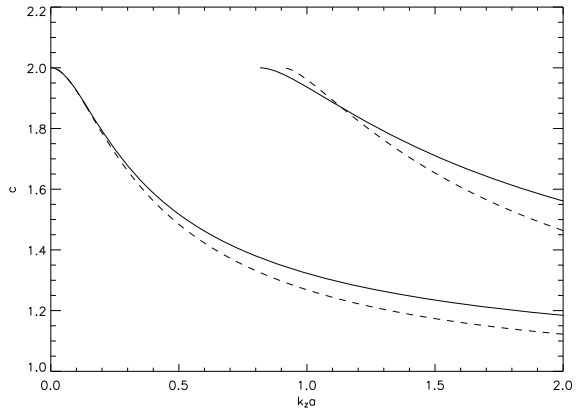

Fig. 7. A plot of the wave speed c (in units of c_{A0}) with respect to $k_z a$ for the Epstein profile (solid curves) and the step function profile (dashed curves), for both kink and sausage modes. Here $c_{Ae}/c_{A0} = 2$ ($\rho_0 = 4\rho_e$).

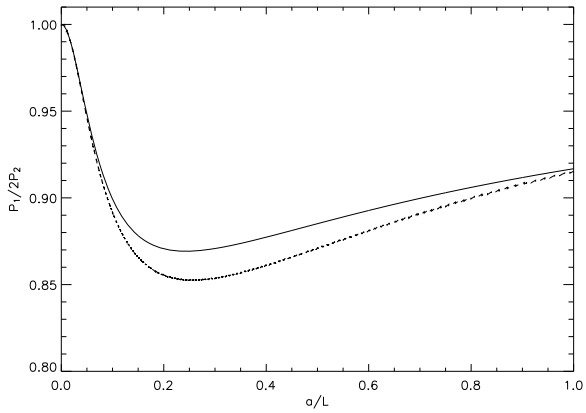

Fig. 8. A plot of the period ratio $P_1/2P_2$ with respect to a/L for the kink mode with an Epstein profile (solid curve) and for the step function profile (dashed curve) for $c_{Ae}/c_{A0} = 2$. Beyond $a/L = 1$, the two curves cross over and later converge together as $a/L \to \infty$.

Thus, we have the dispersion relations (Edwin & Roberts 1982)

$$\cot n_0 a = \frac{n_0}{m_e} \quad \text{and} \quad \tan n_0 a = -\frac{n_0}{m_e} \tag{41}$$

for the kink and sausage modes respectively. Since $\omega = ck_z$ we have

$$\tan\left\{k_z a\left(\frac{c^2 - c_{A0}^2}{c_{A0}^2}\right)^{1/2}\right\} = \frac{c_{A0}}{c_{Ae}}\left(\frac{c_{Ae}^2 - c^2}{c^2 - c_{A0}^2}\right)^{1/2} \tag{42}$$

for the kink mode, and

$$\tan\left\{k_z a\left(\frac{c^2 - c_{A0}^2}{c_{A0}^2}\right)^{1/2}\right\} = -\frac{c_{Ae}}{c_{A0}}\left(\frac{c^2 - c_{A0}^2}{c_{Ae}^2 - c^2}\right)^{1/2} \tag{43}$$

for the sausage mode. The principal kink mode has no cutoff; the cutoff for the principal sausage mode occurs when $c^2 = c_{Ae}^2$ with

$$k_z a = \frac{\pi}{2}\left(\frac{c_{A0}^2}{c_{Ae}^2 - c_{A0}^2}\right)^{1/2}, \quad \text{cutoff}, \tag{44}$$

which may be compared with the cutoff value (30) for the Epstein profile.

Figure 7 gives the behaviour of the wave speed c as a function of $k_z a$, for both the Epstein and step function density profiles.

Figure 8 gives a plot of the period ratio in the kink mode for both the Epstein profile and the step function profile. We note that at $a/L = 1$ the curves are not converging but rather at this point they cross, exhibiting a changeover in behaviour and then converge for $a/L \to \infty$. The period ratio for the sausage mode is shown in Fig. 9. In both cases the period ratio has the same general behaviour, although the period ratio achieves a lower minimum in the step function profile than the Epstein profile, for both kink and sausage modes.

As a final comparison we plot in Figs. 10 and 11 the period ratio for the step function profile for both the kink and sausage modes, for various values of c_{Ae}/c_{A0}. For $c_{Ae}/c_{A0} \to \infty$ the period ratio for the kink mode may be as little as $1/\sqrt{2}$, and for the sausage mode the period ratio may fall to $1/2$. Comparing these plots with Figs. 2 and 5 we note that the limits of $1/\sqrt{2}$ and $1/2$ for the period ratio are the same regardless of whether there is an Epstein profile or a step function profile.

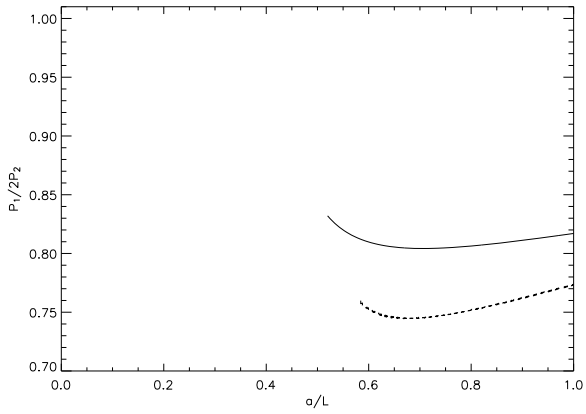

Fig. 9. A plot of the period ratio $P_1/2P_2$ with respect to a/L for the sausage mode with an Epstein profile (solid curve) or for step function profile (dashed curve), for $c_{Ae}/c_{A0} = 2$. Wave cutoff restricts the formation of the period ratio.

6. Discussion

There is a striking similarity between the results for a magnetic slab with Epstein density profile and one with a step function profile. This means that either profile serves as a useful and robust guide as to the expected behaviour in a slab, the Epstein profile perhaps being most useful for numerical investigations with the step function being more readily discussed analytically. Although there are differences in the period ratio from one model to another, it is perhaps unlikely that observations will be able to distinguish between the two cases given the additional complications that other factors, such as longitudinal density and magnetic field variation (see Andries et al. 2009) or non-adiabatic effects (see Macnamara & Roberts 2010) are also likely to impose. Moreover, our assumptions of a slab geometry makes application to flux tube structures problematic.

In future, it would be important to explore the cylindrical case with various density profiles, though it is likely that this would require a largely numerical approach given the expected loss of compact expressions for the wave speed c that a slab geometry provides.

Comparison of our slab results with available observations (such as by Van Doorsselaere et al. 2007, or Srivastava et al. 2008) may be inappropriate until both slab and cylinder results

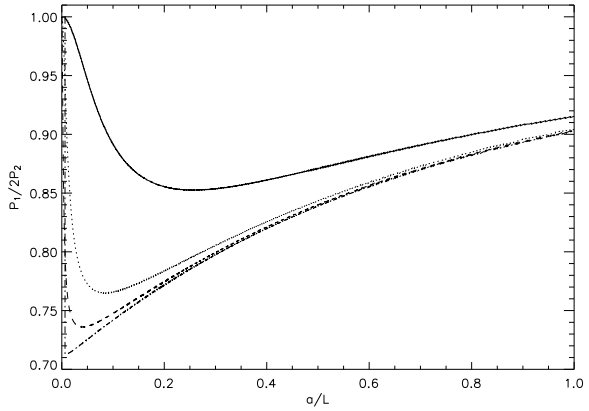

Fig. 10. A plot of the period ratio $P_1/2P_2$ with respect to a/L for the fast kink mode in a step function slab with for $c_{Ae}/c_{A0} = 2, 5, 10$ and 50 for the solid, dotted, dashed and dot-dashed curves respectively.

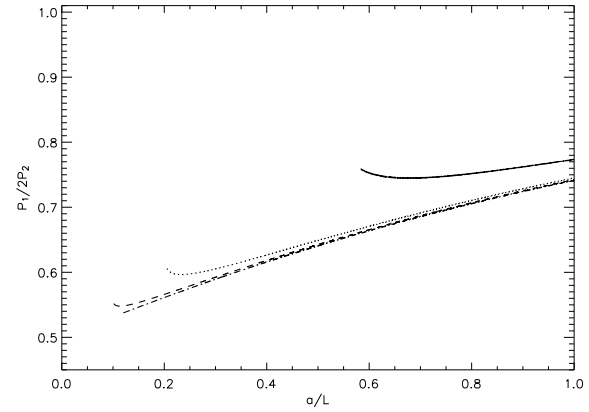

Fig. 11. A plot of the period ratio $P_1/2P_2$ with respect to a/L for the fast sausage mode with step function profile for $c_{Ae}/c_{A0} = 2, 5, 10$ and 50 shown as solid, dotted, dashed and dot-dashed curves respectively. Wave cutoff restricts the formation of the period ratio.

are available, for otherwise it may be that the geometry of a magnetic structure has a larger effect than the lateral profile of density variation.

Acknowledgements. C.K.M. acknowledges financial support from the Carnegie Trust for Scotland. We are grateful to the referee for constructive suggestions which helped improve our paper.

References

Abramowitz, M., & Stegun, I. A. 1965, Handbook of Mathematical Functions
Andries, J., Arregui, I., & Goossens, M. 2005a, ApJ, 624, L57
Andries, J., Goossens, M., Hollweg, J. V., Arregui, I., & Van Doorsselaere, T. 2005b, A&A, 430, 1109
Andries, J., van Doorsselaere, T., Roberts, B., et al. 2009, Space Sci. Rev., 149, 3
Aschwanden, M. J., Fletcher, L., Schrijver, C. J., & Alexander, D. 1999, ApJ, 520, 880
Aschwanden, M. J., de Pontieu, B., Schrijver, C. J., & Title, A. M. 2002, Sol. Phys., 206, 99
Cooper, F. C., Nakariakov, V. M., & Williams, D. R. 2003, A&A, 409, 325
De Moortel, I., & Brady, C. S. 2007, ApJ, 664, 1210
De Moortel, I., Ireland, J., & Walsh, R. W. 2000, A&A, 355, L23
De Moortel, I., Ireland, J., Hood, A. W., & Walsh, R. W. 2002a, A&A, 387, L13
De Moortel, I., Ireland, J., Walsh, R. W., & Hood, A. W. 2002b, Sol. Phys., 209, 61
DeForest, C. E., & Gurman, J. B. 1998, ApJ, 501, L217
Díaz, A. J., Donnelly, G. R., & Roberts, B. 2007, A&A, 476, 359
Donnelly, G. R., Díaz, A. J., & Roberts, B. 2006, A&A, 457, 707
Dymova, M. V., & Ruderman, M. S. 2007, A&A, 463, 759
Edwin, P. M., & Roberts, B. 1982, Sol. Phys., 76, 239
Edwin, P. M., & Roberts, B. 1983, Sol. Phys., 88, 179
Edwin, P. M., & Roberts, B. 1988, A&A, 192, 343
Erdélyi, R., & Morton, R. J. 2009, A&A, 494, 295
Goossens, M., Andries, J., & Arregui, I. 2006, Phil. Trans. R. Soc. A, 364, 433
Inglis, A. R., Van Doorsselaere, T., Brady, C. S., & Nakariakov, V. M. 2009, A&A, 503, 569
Jess, D. B., Mathioudakis, M., Erdélyi, R., et al. 2009, Science, 323, 1582
Landau, L. D., & Lifshitz, E. M. 1958, Fluid Mechanics (Oxford: Pergamon Press)
Macnamara, C. K., & Roberts, B. 2010, A&A, 515, A41
Marsh, M. S., Walsh, R. W., & Plunkett, S. 2009, ApJ, 697, 1674
McEwan, M. P., & De Moortel, I. 2006, A&A, 448, 763
McEwan, M. P., Donnelly, G. R., Díaz, A. J., & Roberts, B. 2006, A&A, 460, 893
McEwan, M. P., Díaz, A. J., & Roberts, B. 2008, A&A, 481, 819
Melnikov, V. F., Reznikova, V. E., Shibasaki, K., & Nakariakov, V. M. 2005, A&A, 439, 727
Morton, R. J., & Erdélyi, R. 2009, A&A, 502, 315
Nakariakov, V. M., & Roberts, B. 1995, Sol. Phys., 159, 399
Nakariakov, V. M., Ofman, L., Deluca, E. E., Roberts, B., & Davila, J. M. 1999, Science, 285, 862
Nakariakov, V. M., Melnikov, V. F., & Reznikova, V. E. 2003, A&A, 412, L7
Ofman, L., & Wang, T. 2002, ApJ, 580, L85
Ofman, L., Romoli, M., Poletto, G., Noci, G., & Kohl, J. L. 1997, ApJ, 491, L111
Ofman, L., Nakariakov, V. M., & DeForest, C. E. 1999, ApJ, 514, 441
O'Shea, E., Srivastava, A. K., Doyle, J. G., & Banerjee, D. 2007, A&A, 473, L13
Pascoe, D. J., Nakariakov, V. M., & Arber, T. D. 2007, A&A, 461, 1149
Pascoe, D. J., Nakariakov, V. M., Arber, T. D., & Murawski, K. 2009, A&A, 494, 1119
Robbrecht, E., Verwichte, E., Berghmans, D., et al. 2001, A&A, 370, 591
Roberts, B. 1981, Sol. Phys., 69, 27
Roberts, B. 2008, in ed. R. Erdélyi, & C. A. Mendoza-Briceño, IAU Symp., 247, 3
Roberts, B., Edwin, P. M., & Benz, A. O. 1984, ApJ, 279, 857
Ruderman, M. S., Verth, G., & Erdélyi, R. 2008, ApJ, 686, 694
Srivastava, A. K., & Dwivedi, B. N. 2010, New Astron., 15, 8
Srivastava, A. K., Zaqarashvili, T. V., Uddin, W., Dwivedi, B. N., & Kumar, P. 2008, Mon. Not. R. Astron. Soc., 388, 1899
Tomczyk, S., & McIntosh, S. W. 2009, ApJ, 697, 1384
Tomczyk, S., McIntosh, S. W., Keil, S. L., et al. 2007, Science, 317, 1192
Van Doorsselaere, T., Nakariakov, V. M., & Verwichte, E. 2007, A&A, 473, 959
Verth, G., & Erdélyi, R. 2008, A&A, 486, 1015
Verwichte, E., Nakariakov, V. M., Ofman, L., & Deluca, E. E. 2004, Sol. Phys., 223, 77
Wang, T. J., & Solanki, S. K. 2004, A&A, 421, L33
Wang, T., Solanki, S. K., Curdt, W., Innes, D. E., & Dammasch, I. E. 2002, ApJ, 574, L101
Wang, T. J., Solanki, S. K., Innes, D. E., Curdt, W., & Marsch, E. 2003, A&A, 402, L17
Wang, T. J., Ofman, L., Davila, J. M., & Mariska, J. T. 2009, A&A, 503, L25